



## Article

# Impacts of Climate Change Induced Sea Level Rise, Flow Increase and Vegetation Encroachment on Flood Hazard in the Biobío River, Chile

Gerhard Schoener <sup>1,\*</sup> , Enrique Muñoz <sup>2,3</sup>, José Luis Arumí <sup>4,5</sup>  and Mark C. Stone <sup>6</sup>

<sup>1</sup> Southern Sandoval County Arroyo Flood Control Authority, 1041 Commercial Dr SE, Rio Rancho, NM 87124, USA

<sup>2</sup> Department of Civil Engineering, Universidad Católica de la Santísima Concepción, Concepción 4030000, Chile

<sup>3</sup> Centro de Investigación en Biodiversidad y Ambientes Sustentables (CIBAS), Universidad Católica de la Santísima Concepción, Concepción 4030000, Chile

<sup>4</sup> Water Resources Department, Faculty of Agricultural Engineering, Universidad de Concepción, Chillan 3812120, Chile

<sup>5</sup> Water Research Center for Agricultural and Mining (CRHIAM), Universidad de Concepción, Concepción 4090541, Chile

<sup>6</sup> Department of Civil, Construction and Environmental Engineering, University of New Mexico, Albuquerque, NM 87131, USA

\* Correspondence: gschoener@sscafca.com

**Abstract:** River flooding is one of the most widespread natural disasters. Projections indicate that climate change will increase flood hazard in many areas around the world. In this study, we investigate the individual and combined effects of sea level rise, flow increase and riparian vegetation encroachment on flood hazard in the lower Biobío River, Chile. Results show that each has the potential to individually increase flood hazard in certain areas, and that individual effects can compound. Encroachment of riparian vegetation onto previously sparsely vegetated areas of the floodplain, likely a result of the Chilean megadrought, causes higher flow resistance and increased flooding during large events. Somewhat counterintuitively, drought has therefore led to an increase in flood hazard in the study area. Drought risk for most land areas across the globe is expected to increase with climate change. Potential future vegetation encroachment should therefore be included as a key variable in riverine flood hazard studies.

**Keywords:** flood hazard; climate change; sea level rise; riparian vegetation encroachment



**Citation:** Schoener, G.; Muñoz, E.; Arumí, J.L.; Stone, M.C. Impacts of Climate Change Induced Sea Level Rise, Flow Increase and Vegetation Encroachment on Flood Hazard in the Biobío River, Chile. *Water* **2022**, *14*, 4098. <https://doi.org/10.3390/w14244098>

Academic Editor: Renato Morbidelli

Received: 9 November 2022

Accepted: 12 December 2022

Published: 15 December 2022

**Publisher's Note:** MDPI stays neutral with regard to jurisdictional claims in published maps and institutional affiliations.



**Copyright:** © 2022 by the authors. Licensee MDPI, Basel, Switzerland. This article is an open access article distributed under the terms and conditions of the Creative Commons Attribution (CC BY) license (<https://creativecommons.org/licenses/by/4.0/>).

## 1. Introduction

River flooding is one of the most widespread natural disasters; between 2000 and 2019, flooding is estimated to account for more than 44% of all natural disasters worldwide, with riverine and flash floods comprising at least three-quarters of all flood events [1]. During the same time span, the number of major floods has more than doubled compared to the previous 20-year period, affecting 1.6 billion people globally [2].

Numerous studies suggest that climate change will increase flood risk [3,4], particularly along rivers in coastal areas [5,6] where rapidly growing population centers with associated economic activity and infrastructure are vulnerable to flooding [7]. Coastal areas are subject to compound flooding, where two or more separate flood drivers such as storm tides and river discharge coincide [5,8,9].

Studies investigating the effect of climate change on compound flooding typically account for the impact of sea level rise and changes in discharge. Kundzewicz et al. [3] analyzed the impact of climate change on river flow, sea level rise and storm surge for a coastal river in Spain and found both to be important factors. Barnard et al. [8] investigated

the compound effect of sea level rise, storms, waves, tides and coastal change on flood hazard exposure in California and found a three-fold increase compared to analyses that only accounted for sea level rise. Bevacqua et al. [6] analyzed the co-occurrence of high sea levels and heavy precipitation in Europe and highlight areas with the highest probability of compound flooding under current and future conditions; they found the compound effect to be worse than the individual occurrence of flood drivers. Kumbier et al. [9] studied the effects of compound flooding due to storm tide and river discharge for a storm in south-east Australia and concluded that by excluding river discharge, flood extent and inundation depths would have been substantially underestimated.

Clearly, the causes of compound flooding must be included in assessments of flood hazard in coastal areas, both under current conditions and when analyzing potential climate change impacts. However, largely missing from the scientific literature is a discussion of the effect of changes in riparian vegetation, which interacts actively with riverine systems [10]. It is well established that shifts in flow regime due to climate change can cause riparian vegetation encroachment into previously unvegetated river channels [11–14]. This, in turn, increases the resistance to flow [15], reduces conveyance [16] and can lead to higher flood stages and thus flood hazard for a given discharge [17]. Nevertheless, shifts in riparian vegetation are usually not included in the analysis of compound flood drivers and warrant further investigation.

The objective of this study was to quantify the impact of climate change, including changes to riparian vegetation, on flood hazards. The lower Biobío River in south-central Chile was chosen as a study case. We analyzed the individual and combined effects of (1) changes in riparian vegetation due to the more than decade-long megadrought, (2) projected sea level rise, and (3) projected increase in discharge during extreme events on flood hazard in the study area. We used a two-dimensional hydrodynamic model (HEC-RAS 2D) and >40 years of historical flow records in our study.

## 2. Data and Methods

### 2.1. Study Area

The Biobío River originates in the Andes of central Chile. With a basin size of more than 24,000 km<sup>2</sup>, it drains the third-largest watershed in the country. This study examines the lower 11 km reach of the Biobío River from the point where it flows into the Gulf of Arauco. The study area encompasses the second-largest metropolitan area in Chile, comprising the cities of Concepción, Hualpén and San Pedro de la Paz (Figure 1) with a combined population of about 1.5 million [18].

Average annual precipitation in the Biobío catchment ranges from more than 4000 mm in the Andes to 1100 mm near the Pacific Ocean. Most of the rainfall is concentrated in the austral (i.e., southern hemisphere) winter, where 5–15 multi-day precipitation events occur each year [19], leading to periodic river flooding. In July of 2006, a frontal system caused massive flooding all over Chile including in the Biobío River system [18], affecting many thousands of residents, damaging property and infrastructure, and disrupting school for more than one month [20]. Numerous other flood events have been documented in the region [21,22].

Figure 2 shows daily discharge measured at the Biobío en Desembocadura gauging station, approximately 10 km upstream from the river mouth. The flow record shows characteristic peaks during the winter months, and generally lower flows throughout the austral summer. Since the year 2010, Chile has experienced persistent drought, with precipitation deficits ranging from 20% to 40% on average [23]. Effects of this so-called megadrought are visible in the flow record of the Biobío River. Average discharge for the 12-year period starting 2010 is 640 m<sup>3</sup> s<sup>-1</sup>, down nearly 40% compared to the period 1970–2009. Winter flow peaks are also markedly lower, less than half compared to the pre-drought period.

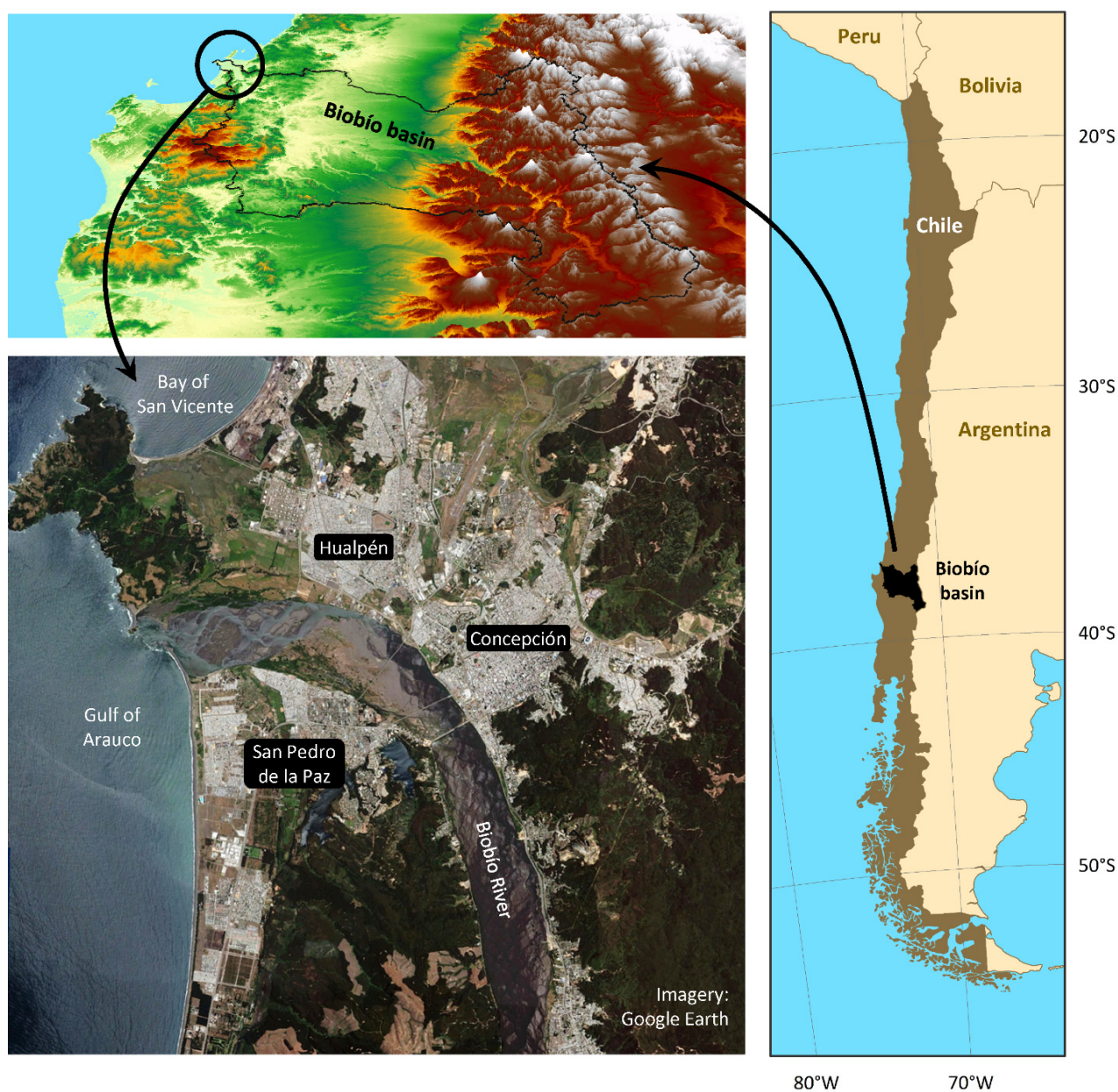


**Figure 1.** Overview map of the study area showing the location of the location of the Biobío River basin in south-central Chile (**right**), a rendering of the topography of the watershed (**top left**), and aerial imagery of the study area showing the lower Biobío River adjacent to the Concepción metropolitan area (**bottom left**) (Images assembled by the authors in ArcGIS using Google Earth imagery and ESRI basemaps).

## 2.2. Hydrodynamic Model

A hydrodynamic model for the study area was built using the US Army Corps of Engineers HEC-RAS 2D software version 6.1. The software was selected because (1) it has built-in geospatial capabilities that can be used to create and manipulate model geometry and analyze results; (2) it is publicly accessible free of charge; (3) it has the capability to use an unstructured computational mesh with associated flexibility to model terrain features; and (4) the model is widely used for flood studies worldwide (see for example [24–26]). A terrain model was developed from lidar-derived elevation data with a spatial resolution of  $2.5 \times 2.5$  m [27] in conjunction with cross-section and bathymetric data for the lower Biobío River [28]. Based on the terrain model, a computational mesh with a spatial resolution of



40 × 40 m was generated in HEC-RAS and refined along channel banks and other important topographic features using breaklines. The model covers an area of approximately 190 km<sup>2</sup> and encompasses the Concepción metropolitan area. Figure S1 (supplementary information) shows a map of the model boundary along with breaklines and cross-section locations. An example of the computational mesh with refinement regions along the banks of the Biobío River can be seen in Figure S2. The hydrodynamic model developed for this study is fully two-dimensional, including areas within the river channel.

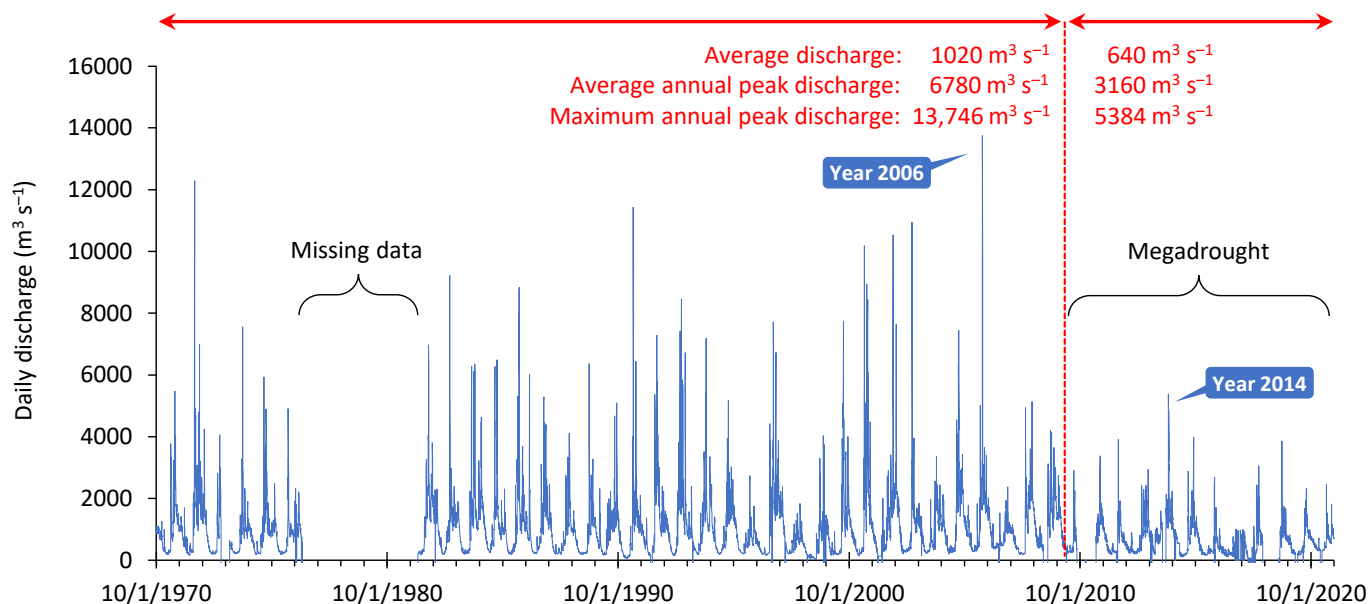


**Figure 2.** Daily discharge measured in the Biobío River at the Desembocadura gauging station approximately 10 km upstream from the confluence with the Pacific Ocean.

### 2.3. Model Boundary Conditions

At the upstream end of the computational domain, a flow boundary condition was used to simulate discharge in the Biobío River. Flow data for the study were obtained from the Dirección General de Aguas (DGA) website (<https://snia.mop.gob.cl/BNAConsultas/reportes>) (accessed on 9 November 2022) for the gauging station Biobío River en Desembocadura, located on the right bank of the river approximately 10 km upstream from the confluence with the Pacific Ocean. Records start in 1970 with a missing period of approximately five years (1977–1981). Hourly discharge measurements are available since 2009; prior data have variable time steps ranging from sub-hourly to several hours in duration. All data were converted to uniform hourly time steps by interpolating between measurements where necessary. Only flows exceeding 6000 m<sup>3</sup> s<sup>−1</sup> are expected to cause overbank flooding in the study area [18]. Thirty-two floods exceeding that threshold were identified from the period of record and used in this analysis (see Table 1). Hourly sea level measurements were obtained from the Servicio Hidrográfico y Oceanográfico de la Armada de Chile (SHOA) for the tide gauge Talcahuano and imposed as downstream boundary conditions.

### 2.4. Comparison of Simulated and Observed Flood Extent for the July 2006 Flood

In July 2006, a warm winter storm caused extreme flooding throughout Chile, including in the study area. The extent of flooding in the greater Concepción area was documented in a series of photographs recorded from an airplane by Didier Rousset Buy close to the time of peak inundation. The 2006 flood was therefore used in this study to compare model results with observed flood extent to assess model performance.

To simulate 2006 conditions, land use in the study area was digitized manually in ArcGIS (ESRI, Redlands, CA, USA) based on Google Earth imagery from the same year. Roughness coefficients (Manning's  $n$ -values) for different land use classes were estimated based on previous work conducted in the study area [18,29] and published guidance [30]. We refer to this as scenario 0. Maps showing  $n$ -values for the 2006 scenario are contained under the supplementary information (Figure S3). Measured discharge was then applied at the upstream model boundary, and simulated flood extent was compared with photographs at strategic locations. Figure 3 shows the maximum extent of inundation based on model results (top, blue) looking south across the study area. The photograph (Figure 3, bottom) shows approximately the same area. For reference, the refinery in Hualpén is outlined in red in both images. Simulated inundation extents for the flood of July 2006 were compared with aerial imagery to assess model performance (see Figure 3 and Figures S4 and S5, Supplementary Information). Visual assessment indicates good agreement between the model and observations. No other data such as surveyed high-water marks or depth measurements were available for model validation.

**Table 1.** Floods analyzed as part of this study, in chronological order.

Number	Date	Peak Flow ( $\text{m}^3 \text{s}^{-1}$ )	Rank
1	5/29/1972	13,110	2
2	8/15/1972	7452	24
3	6/28/1974	9210	10
4	8/18/1982	7083	26
5	6/18/1983	11,082	6
6	5/26/1984	6476	31
7	7/2/1984	6636	30
8	7/18/1984	7040	27
9	5/28/1985	5968	32
10	7/3/1985	8271	20
11	6/18/1986	10,393	8
12	11/27/1986	6938	28
13	6/29/1989	8070	21
14	5/29/1991	12,391	3
15	7/9/1991	7743	23
16	6/6/1992	8412	18
17	6/6/1993	8568	15
18	6/27/1993	8874	12
19	8/28/1993	8433	17
20	7/25/1994	8465	16
21	6/20/1997	8774	13
22	7/30/1997	7158	25
23	8/2/2000	9058	11
24	5/29/2001	10,661	7
25	7/4/2001	10,192	9
26	7/20/2001	8660	14
27	8/2/2001	6756	29
28	8/25/2002	11,124	5
29	10/14/2002	7981	22
30	6/21/2003	12,041	4
31	7/3/2005	8336	19
32	7/12/2006	16,261	1

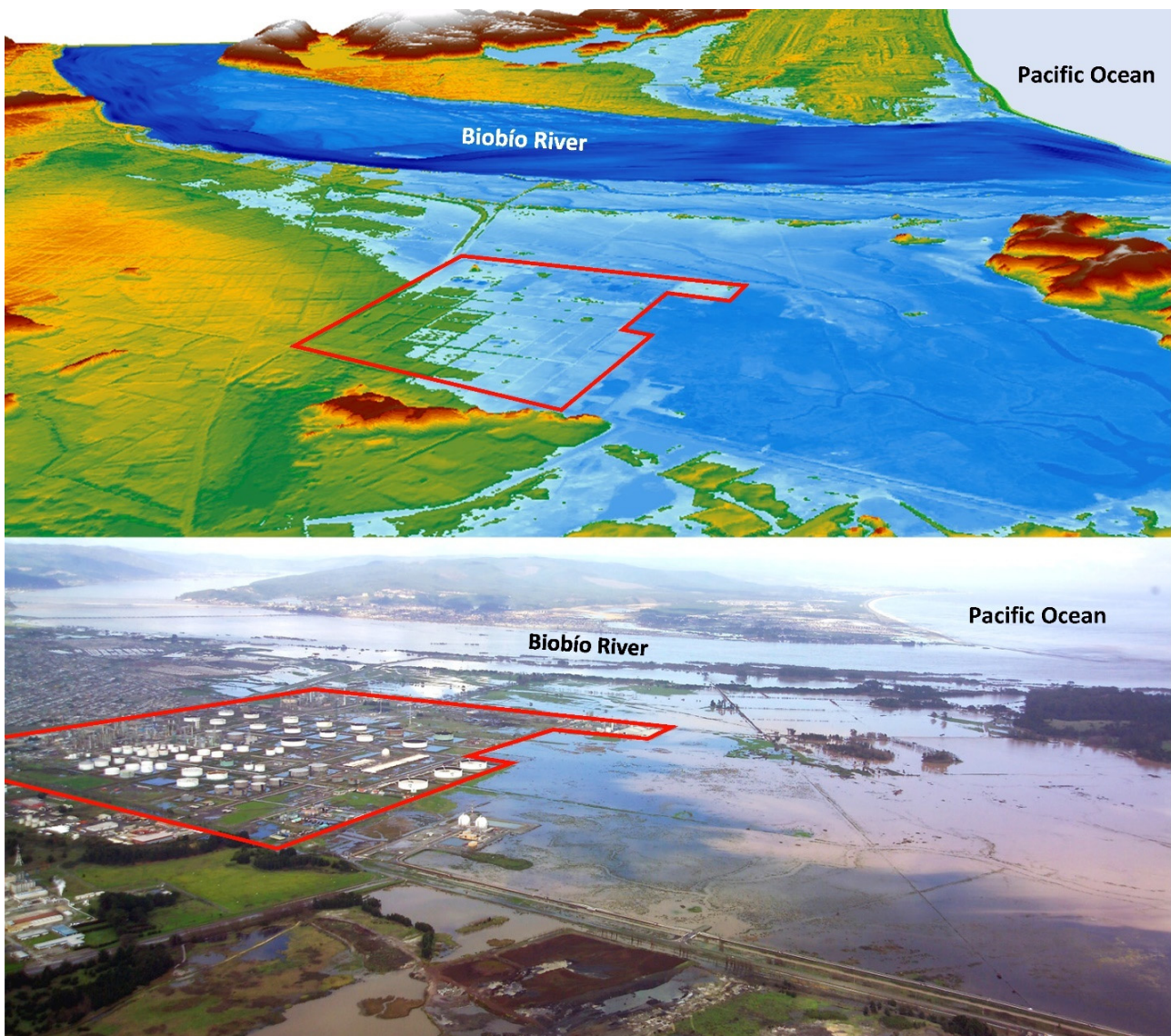


**Figure 3.** Digital elevation model of the study area looking south with simulated flood extent for the July 2006 event (**top**, blue shading), and aerial image of flooding (**bottom**; image source: Didier Rousset Buy). For reference, the location of the refinery north of the Biobío River is indicated with a red outline in both images.

### 3. Model Scenarios

To assess the potential impact of climate change on flooding in the study area, several model scenarios were analyzed. First, a base scenario (scenario 1) was created to characterize current conditions in the study area. Land use for 2022 conditions was digitized from Google Earth imagery, and  $n$ -values were associated with each land use class as described in Section 2.4 (see Table S2 and Figure S3 for  $n$ -values). The base scenario assumes a sandy channel bed with minimal riparian vegetation and a Manning's  $n$ -value of 0.032. 32 historic flood events (see Table 1) were then modeled using corresponding sea level data as the downstream boundary conditions. Results from scenario 1 were used as the benchmark for assessing changes related to three distinct climate change impacts: (1) sea level rise, (2) change in channel vegetation, and (3) changes in river flow. Table 2 contains a summary of assumptions for each scenario. Justifications for each assumption are discussed below.



**Table 2.** Summary of model scenarios and underlying assumptions for sea level rise, discharge and riparian vegetation.

Description	Model Scenario	Sea Level	Discharge	Riparian Vegetation
Calibration	0	measured sea levels	measured discharge	2006 conditions
Base scenario	1	measured sea levels	measured discharge	channel $n = 0.032$
	2	sea levels +0.3 m	measured discharge	channel $n = 0.032$
Impact of sea level rise	3	sea levels +0.6 m	measured discharge	channel $n = 0.032$
	4	sea levels +0.9 m	measured discharge	channel $n = 0.032$
Impact of channel vegetation	5	measured sea levels	measured discharge	sand bar $n = 0.032$ –0.140
	6	measured sea levels	measured discharge	sand bar $n = 0.070$ –0.160
Impact of discharge increase	7	measured sea levels	discharge + 7%	channel $n = 0.032$
	8	measured sea levels	discharge + 11%	channel $n = 0.032$
	9	measured sea levels	discharge + 18%	channel $n = 0.032$
Worst case scenario	10	sea levels +0.9 m	discharge + 18%	sand bar $n = 0.070$ –0.160

### 3.1. Sea Level Rise

Based on the sixth assessment report by the Intergovernmental Panel on Climate Change [31], the expected mean sea level rise for the East Pacific is between 0.3 and 0.9 m by the end of this century, depending on emissions scenario. Given this projection, we modeled three sea level scenarios, increasing historic hourly sea level data for the 32 flood events analyzed in this study by 0.3 m, 0.6 m and 0.9 m, respectively (see Table 2, scenarios 2–4). Like the base scenario, sea level scenarios assume a sandy channel bed with minimal riparian vegetation (see Figure S3).

### 3.2. Change in Riparian Vegetation

Review of aerial photographs and field investigation conducted by the authors in 2022 reveal that vegetation on a large sand bar present on the south side of the channel has increased substantially over the past 20 years (see Figure 4). Establishment of vegetation—including a dense riparian forest near the south bank that gradually transitions to shrub and scrub vegetation towards the active channel—has likely been promoted by the lack of high flows during the more than decade-long megadrought (see Figure 2).

To assess the impact of vegetation growing in the channel, the sand bar was divided into four distinct vegetation zones (see Figure 5). Two vegetation scenarios were then analyzed: scenario 5, with sand ( $n = 0.032$ ), scrubland ( $n = 0.07$ ), shrub ( $n = 0.12$ ) and forest ( $n = 0.14$ ) occupying zones 1–4, respectively. This is representative of the conditions encountered in the field in 2022. Future scenario 6 assumes that even more of the sand bar is covered in vegetation: scrub ( $n = 0.07$ ), shrub ( $n = 0.12$ ), forest ( $n = 0.14$ ) and dense riparian forest ( $n = 0.16$ ) covering zones 1–4, respectively.

### 3.3. Increase in Discharge

According to the 2022 IPCC report [31], by mid-century, 50-year peak flows in central Chile are expected to be greater than 100-year peak flows observed over the reference period [6]. Based on annual discharge maxima for the available period of record, we estimated flood frequency for the lower Biobío River as outlined in USGS Bulletin 17 [32] using HEC-SSP software version 2.2. A table containing recurrence intervals and associated flow rates is contained under supplementary information (Table S1). Results show that based on historic observations, the 1% exceedance chance (100-year recurrence interval) peak discharge is  $15,715 \text{ m}^3 \text{ s}^{-1}$  (95% CI: 22,784–12,722  $\text{m}^3 \text{ s}^{-1}$ ), and the 2% exceedance chance (50-year recurrence interval) peak flow is  $14,184 \text{ m}^3 \text{ s}^{-1}$  (95% CI: 19,267–11,838  $\text{m}^3 \text{ s}^{-1}$ ). The difference between the 50-year and 100-year recurrence intervals is 11% (7–18% for the 95% confidence interval). In accordance with this analysis, we modeled three scenarios that account for potential increases in discharge due to climate change by increasing measured

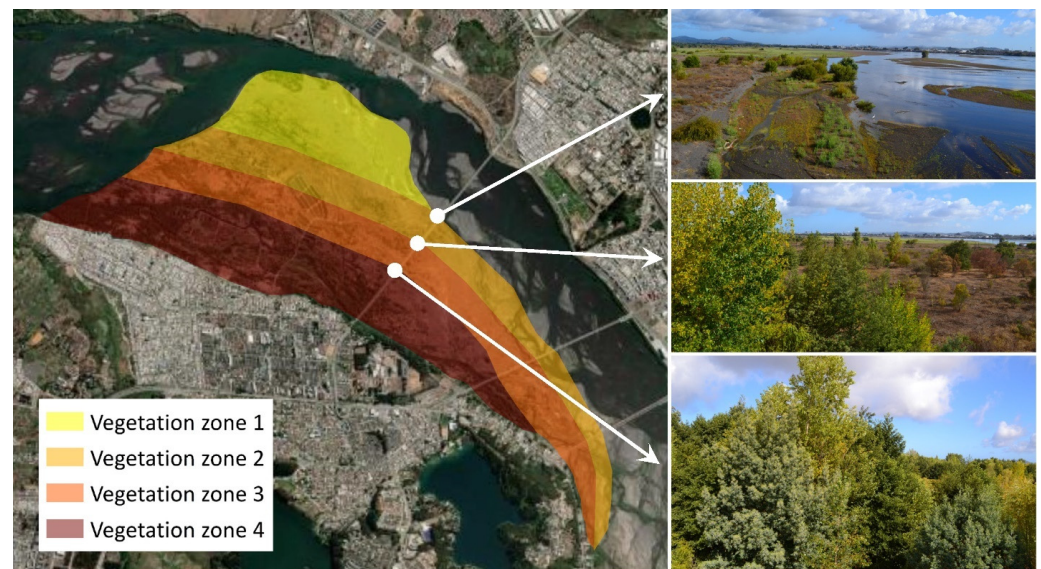
flood hydrographs for all 32 events listed in Table 1 by 7%, 11% and 18% (scenarios 7, 8 and 9, respectively).

Scenarios 2–9 shed light on potential effects of sea level rise (scenarios 2–4), shift in riparian vegetation (scenarios 5 and 6), and peak flow increase (scenarios 7–9), respectively. In addition, we modeled a worst-case scenario (10) with maximum sea level rise (+0.9 m), maximum sand bar vegetation, and maximum peak flow increase (+18%) to assess compounding effects.



**Figure 4.** Imagery from 2002 (**top**), 2012 (**center**) and 2022 (**bottom**) showing vegetation changes on the sand bar in the lower Biobío River (image source: Google Earth).

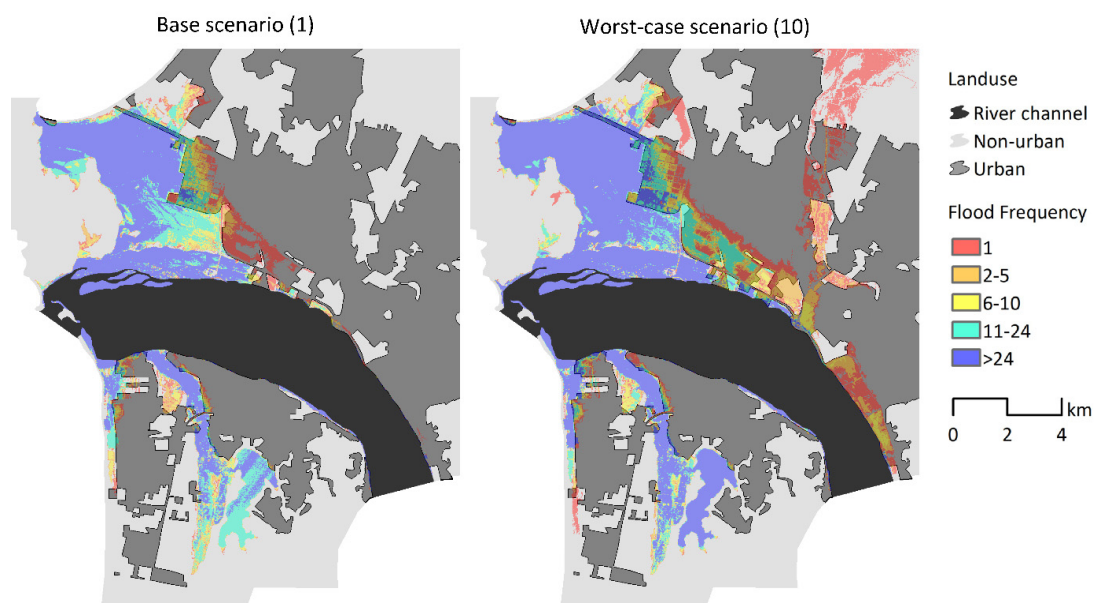




**Figure 5.** Map showing the sand bar in the lower Biobío River (left, image source: Google Earth), and photos at the transition of different vegetation zones (looking downstream) taken by the authors in February 2022.

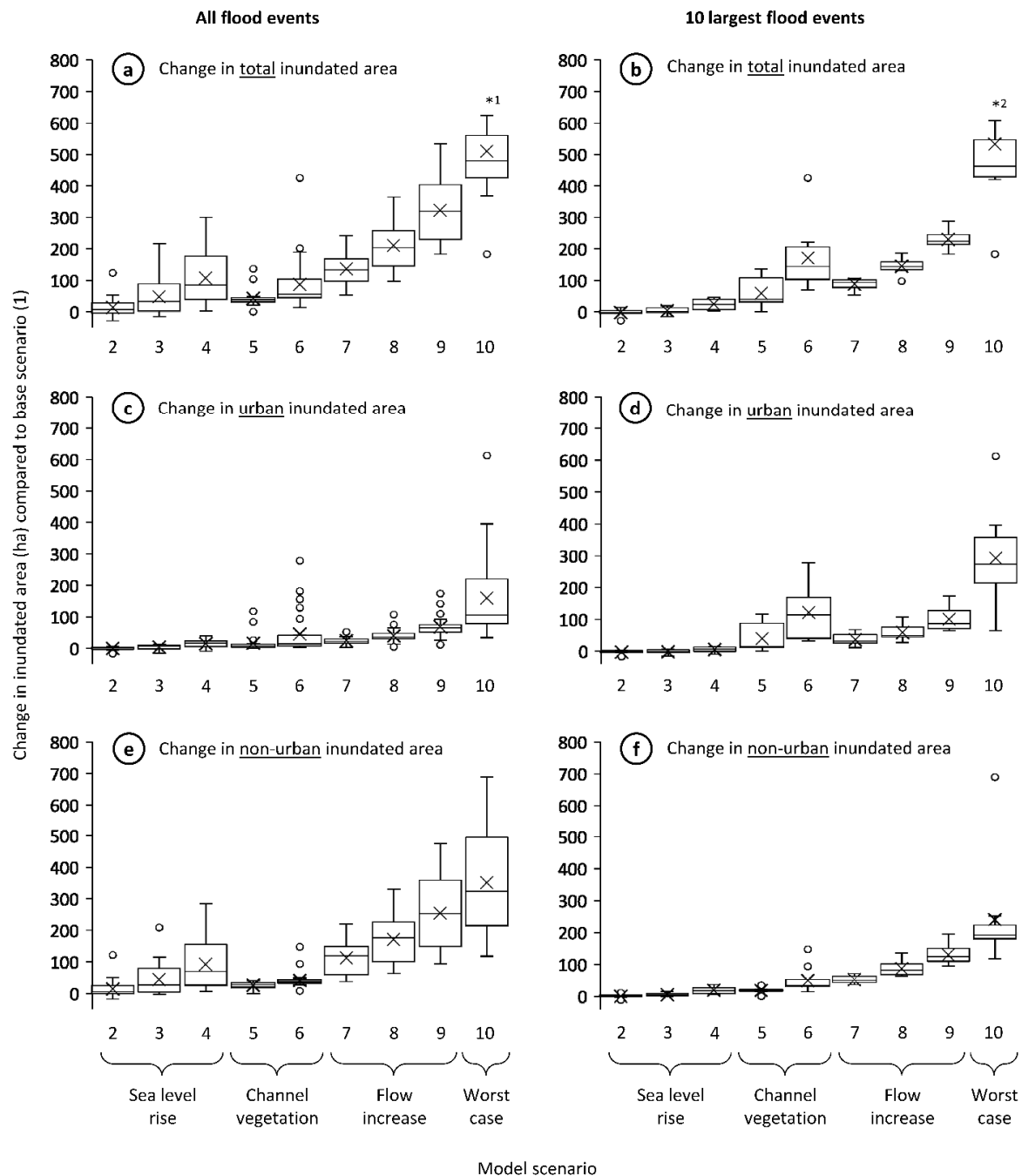
#### 4. Results

Figure 6 shows the frequency of inundation in the study area based on the 32 observed flood events analyzed in this study for scenario 1 (base scenario, left) and scenario 10 (worst-case, right). Urbanized areas in 2022 are shown with a dark gray background, and the river channel is displayed in black. Frequency of flooding in Figure 6 relates to all 32 flood events modeled as part of this study. For example, areas shaded in red were inundated by 1 of 32 events, while areas shaded in blue were inundated during more than 24 out of 32 floods. Flood frequency maps for the remaining scenarios are contained under Supplementary Information (Figures S6 and S7). A marked increase in flood frequency is evident for the worst-case scenario, particularly in urban areas north of the river channel.



**Figure 6.** Maps showing frequency of flooding in the study area based on 32 flood events for the base scenario (1, left) and the worst-case scenario (10, right). The river channel is indicated with black shading; areas urbanized in 2022 are indicated with a darker shade of gray.

The base scenario (1) was then used to assess the change in inundated area for scenarios 2–10. Figure 7 contains boxplots for each scenario showing the change in total inundated area (top) compared to scenario 1, and separately for urbanized area (center) and non-urbanized area (bottom). The left column contains results for all 32 floods, while the column on the right shows results for only the ten largest events (i.e., flows exceeding  $9200 \text{ m}^3 \text{ s}^{-1}$ ). Varying climate change impacts on flood extent are apparent.



Outliers not shown on charts: \*1 1302 ha; \*2 1302 ha

**Figure 7.** Box plots showing change in inundated area (ha) for scenarios 2–10 compared to the base scenario (1), for total area (top, panels a,b), urbanized area (center, panels c,d), and non-urbanized area (bottom, panels e,f). Results for all 32 floods are shown on the left (panels a,c,e), and results for the ten largest floods are displayed on the right (panels b,d,f).

Comparing data for all floods and total area (Figure 7, panel a), the largest increase in flood extent can be observed for the worst-case scenario (10), followed by peak flow increase (scenarios 7–9) and sea level rise of 0.6 and 0.9 m (scenarios 3 and 4). Scenario 2 (0.3 m sea level rise) and vegetation scenarios (5 and 6) appear to have a lesser impact, with the exception of one outlier for scenario 6.

Evaluation of model results revealed that impacts of sea level rise and vegetation encroachment vary with flood magnitude. The right-hand side of Figure 7 therefore shows change in inundated area for the largest ten flood events only. It is apparent that increases in riparian vegetation (scenarios 5 and 6) have a large impact on flood extent for the largest discharges (i.e., flows exceeding  $9200 \text{ m}^3 \text{ s}^{-1}$ ), particularly in the urbanized area (panel d). Sea level rise, on the other hand, minimally increases flood extent during large floods. The impact of sea level rise is most apparent for non-urban areas when all events are considered (panel e). Figure 7 illustrates that more than 600 ha of urbanized area are vulnerable to flooding under worst-case conditions (see Figure 7c); this is in addition to portions of the Concepción metropolitan area already at risk of flooding under current (2022) conditions.

Figure 8 shows the impact of individual climate change effects on maximum flood extent during the smallest event analyzed in this study (flood 9, peak flow =  $5968 \text{ m}^3 \text{ s}^{-1}$ ). In each panel, flood extent resulting from the base scenario is shaded in blue. Panel a shows the increase in flood extent (yellow) due to 0.9 m sea level rise (scenario 4). Sea level rise mostly impacts the low-lying portion of the study area near the river mouth and along wetlands north and south of the channel. The Concepción metropolitan area has experienced substantial population growth over the last decades [18,22], and many of the new urban areas occupy former wetlands [33]. Panel b shows the increase in flood extent due to maximum riparian vegetation (scenario 6). During small flood events, riparian vegetation encroachment only leads to a slight increase in flood extent along the banks of the river (red shading, Figure 8b). Finally, purple shading in panel c illustrates the effects of 18% increase in discharge (scenario 9). Similar to the sea level rise scenario, areas most affected by flow increase during small floods are low-lying wetlands in the lower portion of the study area.

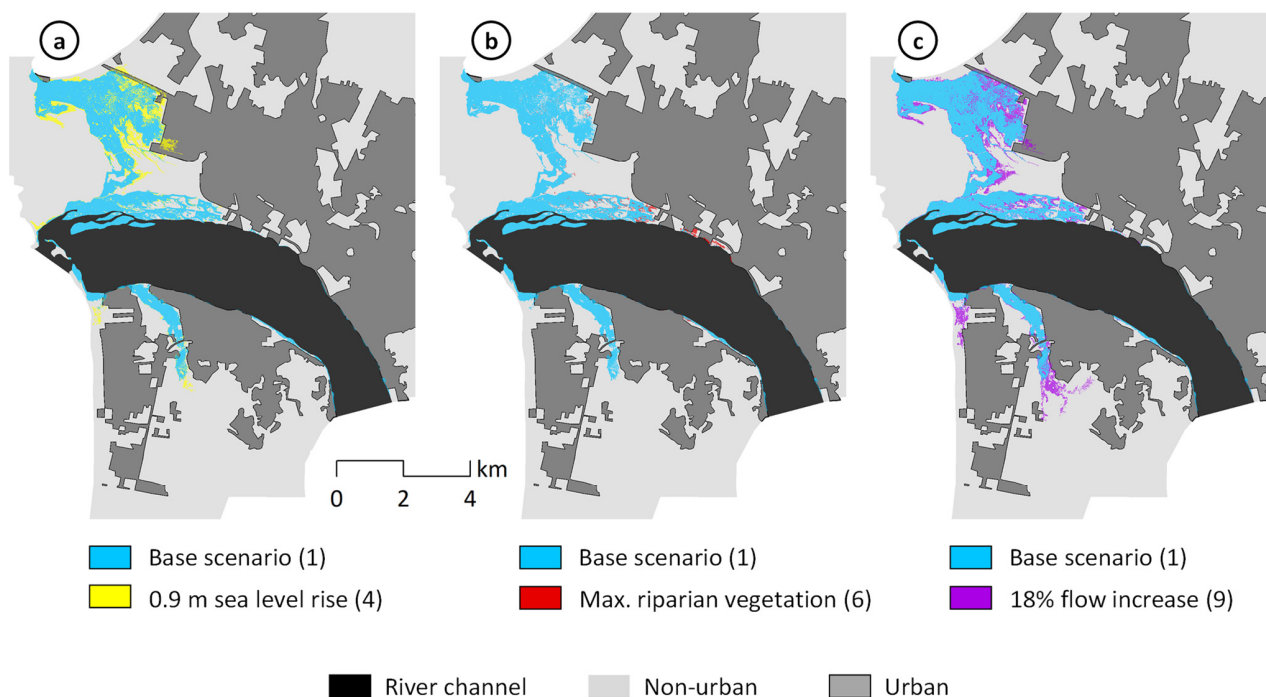


**Figure 8.** Maps showing differences in flood extent between the base scenario (1, blue) and scenarios 4 (yellow, panel a), 6 (red, panel b) and 9 (purple, panel c) for the flood with the smallest peak flow rate analyzed in this study (event 9, peak flow =  $5968 \text{ m}^3 \text{ s}^{-1}$ ).



Figure 9 contains the same comparison, but this time for the largest flood event observed during the study period (flood 32, peak flow =  $16,261 \text{ m}^3 \text{ s}^{-1}$ ). Lack of yellow shading in panel d illustrates that during large floods, sea level rise has practically no impact of flood extent in the study area. In contrast, riparian vegetation encroachment substantially increases flood extent (red shading, Figure 9, panel e). Increase in woody vegetation on the sand bar in the Biobío River causes higher resistance to flow and therefore greater flow depths for a given discharge. During large events, this causes floodwaters to leave the channel and inundate urban areas to the north. Assuming heavy vegetation on the sand bar (scenario 6), the model predicts that an old river channel that now crosses downtown Concepción would have been activated during the 2006 flood (event 32). Remnants of the channel are still visible in the satellite image in Figure 1. Increase in discharge results in larger flood extent (purple shading, Figure 9 f) throughout the study area during large flows. Figures 8 and 9 illustrate how changes to flood hazard due to sea level rise, flow increase and riparian vegetation encroachment are dependent on local topography and proximity to downstream boundary conditions. Moreover, impacts vary with flood magnitude. In the study area, sea level rise is expected to cause a notable increase in flood extent during small events, while having a negligible impact during the largest floods. The opposite is true for riparian vegetation encroachment, which is anticipated to increase flood extent during large events while having minimal impact during smaller floods.

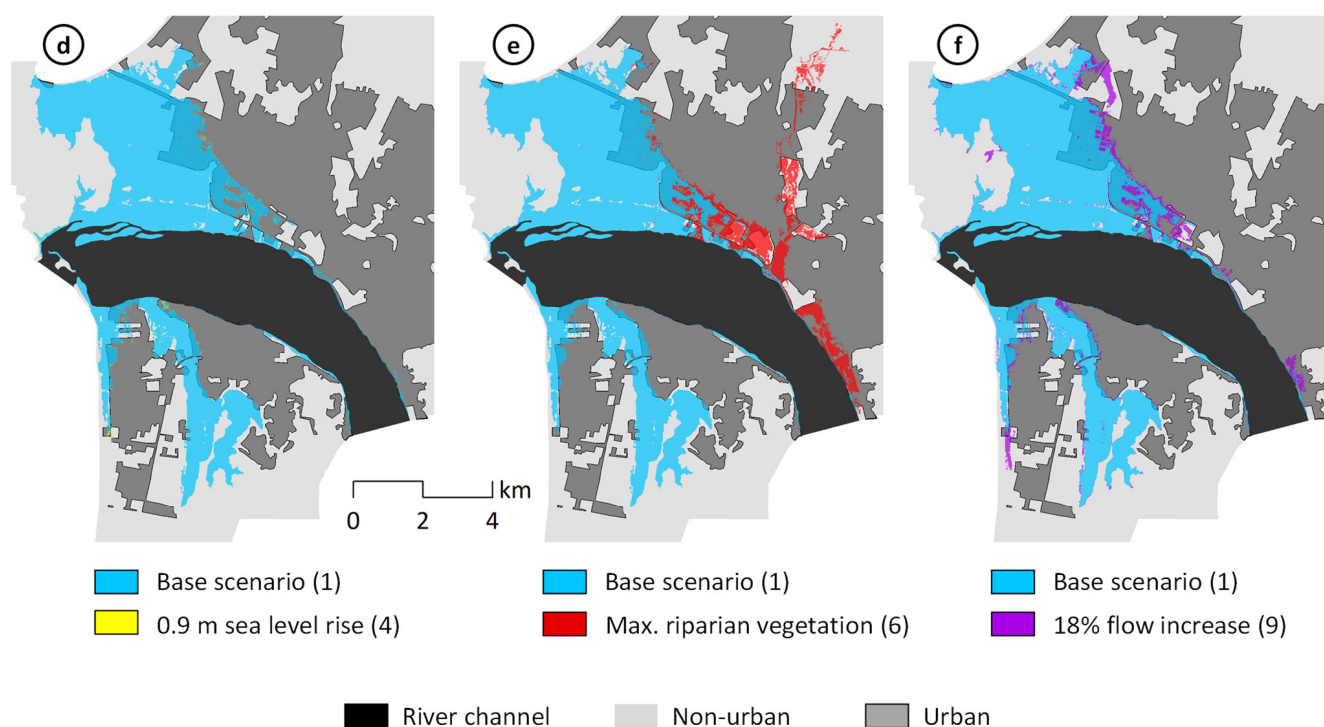


**Figure 9.** Maps showing differences in flood extent between the base scenario (1, blue) and scenarios 4 (yellow, panel d), 6 (red, panel e) and 9 (purple, panel f) for the flood with the largest peak flow rate analyzed in this study (flood event 32, peak flow =  $16,261 \text{ m}^3 \text{ s}^{-1}$ ).

## 5. Discussion

Flood hazard is one component of flood risk, which is composed of hazard, exposure and vulnerability [3,34]. Exposure and vulnerability are not addressed in this study and are identified as an important area of future investigation. We evaluated flood hazard based on observations from a gauging station located in the study area. Underlying this approach is the assumption that the discharge record encompasses most of the historical variability of the system. This assumption appears justified given the length of the record (>40 years). Using historical observations as a baseline, we assessed the individual and

combined impacts of climate change–induced sea level rise, flow increase and riparian vegetation encroachment. Other potential flood drivers in coastal areas such as tsunamis and storm surge were not included in the analysis; this is a limitation of the present study. Simulated inundation extents for the flood of July 2006 were compared with aerial imagery recorded during the event. Visual assessment indicates good agreement between model and observations. Ideally, surveyed high-water marks or depth measurements would be used to evaluate model performance, but no such records were available for model validation.

The computational mesh for the hydrodynamic model was developed based on topographic data with high spatial resolution collected in 2010. A large earthquake in February of 2010 reportedly caused both areas of uplift and subsidence along the Chilean coast and may have impacted land levels in the study area [35]. Since flood extent is dependent on topography, subsidence may increase flood hazard, while the opposite is true for areas of uplift. Surveyed cross-sections and bathymetry used in this study were collected after the earthquake, but the digital elevation model used for areas outside of the river channel predates the earthquake. No other dataset with the same spatial resolution was available to the authors. In areas where the land surface has changed, results may not be representative of current conditions.

Limitations in available data for model development and validation contribute to model uncertainty. Despite those limitations, the study provides valuable insights into the relative changes to flood extent caused by climate change, as well as the connection between flood magnitude and climate change–induced flood hazard. Results show that effects on flood extent are highly dependent on location due to local topography, proximity to downstream boundary conditions, as well as riparian vegetation dynamics; this makes generalization challenging. Nevertheless, three broad conclusions can be drawn: (1) all three climate change effects—sea level rise, flow increase and the increase in channel vegetation—have the potential to individually increase flood hazard in certain areas; (2) individual effects can compound; (3) effects of sea level rise and vegetation encroachment vary with flood magnitude.

Sea level rise mostly impacts the low-lying portion of the study area near the river mouth and along wetlands north and south of the channel. Over the past decades, the Concepción metropolitan area has experienced substantial population growth [18,22]. Land available for urbanization is limited, and much of the new construction occupies former wetlands [33]. These low-lying areas will flood more frequently with increasing sea levels. Coastal wetlands provide numerous ecosystem services, among them protection from tsunami damage and storm surge. The role of this important ecosystem service has been demonstrated in portions of the study area [33] and for coastal wetlands worldwide [36]. Wetland protection should therefore be seen as a priority—both to preserve important ecosystem services, and because these low-lying areas will flood more frequently in future decades.

Riparian vegetation encroachment has a large impact on flood extent in the urbanized area north of the river channel, particularly during large flood events. Riparian vegetation varies in space and time in response to river flow [11]. Shifts in flow regime due to climate change or river regulation can cause riparian vegetation encroachment [11–14]. Large floods uproot vegetation [37], while frequent flooding creates bare substrates within the channel [38]. When the frequency and magnitude of flooding decreases, riparian plants encroach onto previous unvegetated areas of the floodplain [39–41]. This can lead to bed incision [42], channel narrowing [43] and an increase in flood hazard due to increased channel roughness [15].

The drastic increase in vegetation on the sand bar that can be observed for the 20-year period 2002–2022 in the study area (see Figure 4) is likely related to the more than decade-long megadrought Chile has been experiencing [23]. Before the drought, which started in 2010, periodic high flows (see Figure 2) would scour the channel and remove large vegetation. After 2010, annual average peak discharge decreased to less than half of the pre-drought record. Similar patterns can be observed in other Chilean rivers. Pacheco et al. [44]

reported increases in riparian vegetation for the Maule River in central Chile and attributed changes to operation of a hydropower dam as well as the Chilean megadrought. Batalla et al. [45] examined a segment of the free-flowing River Ñuble in the Mediterranean portion of Chile and likewise reported riparian vegetation encroachment related to a reduction in the magnitude and frequency of flood events. Images illustrating the encroachment of riparian vegetation at the confluence of the Ñuble and Itata rivers are included under supplementary information (see Figure S8).

Healthy riparian vegetation is essential for the function of river ecosystems [13]; nevertheless, encroachment of riparian plants onto previously unvegetated areas of the channel can have negative consequences. This study demonstrates that prolonged drought—exacerbated by climate change—and lack of periodic high flow events can lead to riparian vegetation encroachment, increased roughness and, consequently, overbank flooding. Somewhat counterintuitively, drought can therefore lead to an increase in flood hazard. Drought risk is expected to rise for most land areas across the globe, and particularly large increases are projected for Africa and South America [46]. Projected effects on river corridors include channel narrowing and vegetation encroachment [11,17,47]. Potential impacts of vegetation encroachment should therefore be included as a key variable in riverine flood hazard studies.

## 6. Conclusions

In this study, we evaluated the effect of climate change on flood hazard in the lower Biobío River (Concepción metropolitan area, Chile). Specifically, we assessed the individual and combined impacts of sea level rise, flow increase and riparian vegetation encroachment. Results show that each has the potential to individually increase flood hazard in certain areas, and that individual effects can compound. Sea level rise mainly impacts low-lying areas (wetlands, salt marshes) during more frequent floods; these areas have experienced an increase in urbanization over the past decades and are projected to flood more frequently with rising sea levels compounded by projected increases in peak flows. Encroachment of riparian vegetation onto previously sparsely vegetated areas of the floodplain causes higher resistance to flow and increases flood hazard during large events; this may also be exacerbated by projected increases in peak discharge. Vegetation encroachment is likely related to the more than decade-long megadrought in the study area. The drought has led to a reduction in the frequency and magnitude of flood events and allowed establishment of large woody vegetation on the floodplain. Somewhat counterintuitively, the drought has therefore led to an increase in flood hazard in the study area. Similar patterns of riparian vegetation encroachment can be observed for other Chilean rivers. Since drought risk is expected to increase in South America and globally, potential future vegetation encroachment should be included as a key variable in riverine flood hazard studies.

**Supplementary Materials:** The following supporting information can be downloaded at: <https://www.mdpi.com/article/10.3390/w14244098/s1>, Figure S1: Map of the study area showing the boundary of the hydrodynamic model (blue), breaklines used to refine the computational mesh (red), and locations of surveyed cross-sections (yellow); Figure S2: Detailed view of a portion of the computational mesh (blue) and refinement regions along the banks of the Biobío River (red); Figure S3: Manning's  $n$ -values for different model scenarios; Figure S4: Overview map (top) showing locations where modeled and observed flood extent for the 2006 flood were compared, and comparison at location 1 (bottom; see red line for comparison); Figure S5: Comparison of modeled (left) and observed flood extents (right) at locations 2, 3 and 4 (see red line for comparison); Figure S6: Maps showing frequency of flooding in the study area based on 32 flood events for scenarios 2–5. The river channel is indicated with black shading; areas urbanized in 2022 are indicated with a darker shade of grey; Figure S7: Maps showing frequency of flooding in the study area based on 32 flood events for scenarios 6–9. The river channel is indicated with black shading; areas urbanized in 2022 are indicated with a darker shade of grey; Figure S8: Photos showing the confluence of the Ñuble and Itata Rivers (Latitude:  $-36.642239^\circ$ , Longitude:  $-72.466197^\circ$ ) in central Chile in 2006, 2009, 2013 and 2022 (image source: José Luis Arumí); Table S1: Calculated recurrence intervals and associated peak flows and 95% confidence limits for



the lower Biobío River based on annual maximum time series using the method outlined in USGS Bulletin 17; Table S2: Manning's  $n$ -values for different land use types.

**Author Contributions:** Conceptualization and methodology: G.S., E.M., J.L.A. and M.C.S.; Formal analysis and investigation: G.S.; Writing—original draft preparation: G.S.; Writing—review and editing: G.S., E.M., J.L.A. and M.C.S. All authors have read and agreed to the published version of the manuscript.

**Funding:** This work was supported by the National Science Foundation (grants number 1954140 and 1826709) and by the CRHIAM Center, project ANID/FONDAP/15130015.

**Institutional Review Board Statement:** Not applicable.

**Informed Consent Statement:** Not applicable.

**Data Availability Statement:** The authors mainly relied on publicly available software (U.S. Army Corps of Engineers) and data from the Dirección General de Aguas (DGA), the Servicio Hidrográfico y Oceanográfico de la Armada de Chile (SHOA), and Google Earth. River cross-sections and bathymetry were obtained from the Ministerio de Obras Públicas. The lidar-derived digital elevation model was obtained from the Universidad del Biobío. Hydrodynamic models developed as part of this study are available from the corresponding author upon request.

**Acknowledgments:** This study was supported by the Partnerships Along the Headwaters of the Americas for Young Scientists (Pathways) program, an international research experience for students funded by the National Science Foundation (grant number 1954140) and hosted by Washington State University and the University of New Mexico. Special thanks to Mark Stone, Asa Stone, Jan Boll, Benjamin Warner and Alex Fremier for making the experience possible despite many setbacks during the COVID-19 pandemic. We are also grateful to the Centro de Investigación Marítimo Portuario—CIMP UCSC for providing the lidar-based digital elevation model used in this project. Additional funding was provided by the CRHIAM Center, project ANID/FONDAP/15130015.

**Conflicts of Interest:** The authors declare no conflict of interest.

## References

1. CRED. Centre for Research on the Epidemiology of Disasters (CRED). EM-DAT: The International Disaster Database. Université Catholique de Louvain, Brussels, Belgium. 2022. Available online: <https://www.emdat.be/> (accessed on 13 April 2022).
2. United Nations Office for Disaster Risk Reduction (UNDRR). *The Human Cost of Disasters: An Overview of the Last 20 Years (2000–2019)*; UNDRR: Geneva, Switzerland, 2020.
3. Kundzewicz, Z.W.; Su, B.; Wang, Y.; Wang, G.; Wang, G.; Huang, J.; Jiang, T. Flood risk in a range of spatial perspectives—from global to local scales. *Nat. Hazards Earth Syst. Sci.* **2019**, *19*, 1319–1328. [\[CrossRef\]](#)
4. Tanoue, M.; Hirabayashi, Y.; Ikeuchi, H. Global-scale river flood vulnerability in the last 50 years. *Sci. Rep.* **2016**, *6*, 36021. [\[CrossRef\]](#)
5. Bermúdez, M.; Farfán, J.F.; Willems, P.; Cea, L. Assessing the Effects of Climate Change on Compound Flooding in Coastal River Areas. *Water Resour. Res.* **2021**, *57*, e2020WR029321. [\[CrossRef\]](#)
6. Bevacqua, E.; Maraun, D.; Voudoukas, M.I.; Voukouvalas, E.; Vrac, M.; Mentaschi, L.; Widmann, M. Higher probability of compound flooding from precipitation and storm surge in Europe under anthropogenic climate change. *Sci. Adv.* **2019**, *5*, eaaw5531. [\[CrossRef\]](#)
7. Koks, E.E.; Jongman, B.; Husby, T.G.; Botzen, W.J. Combining hazard, exposure and social vulnerability to provide lessons for flood risk management. *Environ. Sci. Policy* **2015**, *47*, 42–52. [\[CrossRef\]](#)
8. Barnard, P.L.; Erikson, L.H.; Foxgrover, A.C.; Hart, J.A.F.; Limber, P.; O'Neill, A.C.; Van Ormondt, M.; Vitousek, S.; Wood, N.; Hayden, M.K.; et al. Dynamic flood modeling essential to assess the coastal impacts of climate change. *Sci. Rep.* **2019**, *9*, 4309. [\[CrossRef\]](#)
9. Kumbier, K.; Carvalho, R.C.; Vafeidis, A.T.; Woodroffe, C.D. Investigating compound flooding in an estuary using hydrodynamic modelling: A case study from the Shoalhaven River, Australia. *Nat. Hazards Earth Syst. Sci.* **2018**, *18*, 463–477. [\[CrossRef\]](#)
10. Solari, L.; Van Oorschot, M.; Belletti, B.; Hendriks, D.; Rinaldi, M.; Vargas-Luna, A. Advances on modelling riparian vegetation—hydromorphology interactions. *River Res. Appl.* **2016**, *32*, 164–178. [\[CrossRef\]](#)
11. Diehl, R.M.; Wilcox, A.C.; Stella, J.C. Evaluation of the integrated riparian ecosystem response to future flow regimes on semiarid rivers in Colorado, USA. *J. Environ. Manag.* **2020**, *271*, 111037. [\[CrossRef\]](#)
12. Diehl, R.M.; Wilcox, A.C.; Merritt, D.M.; Perkins, D.W.; Scott, J.A. Development of an eco-geomorphic modeling framework to evaluate riparian ecosystem response to flow-regime changes. *Ecol. Eng.* **2018**, *123*, 112–126. [\[CrossRef\]](#)
13. Durning, L.E.; Sankey, J.B.; Yackulic, C.B.; Grams, P.E.; Butterfield, B.J.; Sankey, T.T. Hydrologic and geomorphic effects on riparian plant species occurrence and encroachment: Remote sensing of 360 km of the Colorado River in Grand Canyon. *Ecohydrology* **2021**, *14*, e2344. [\[CrossRef\]](#)

14. Webb, R.H.; Leake, S.A.; Turner, R.M. *The Ribbon of Green: Change in Riparian Vegetation in the South-Western United States*; University of Arizona Press: Tucson, AZ, USA, 2007.
15. Darby, S.E. Effect of Riparian Vegetation on Flow Resistance and Flood Potential. *J. Hydraul. Eng.* **1999**, *125*, 443–454. [\[CrossRef\]](#)
16. Wang, C.; Zheng, S.-S.; Wang, P.-F.; Hou, J. Interactions between vegetation, water flow and sediment transport: A review. *J. Hydrodyn.* **2015**, *27*, 24–37. [\[CrossRef\]](#)
17. Kiss, T.; Nagy, J.; Fehérvári, I.; Vaszkó, C. (Mis) management of floodplain vegetation: The effect of invasive species on vegetation roughness and flood levels. *Sci. Total Environ.* **2019**, *686*, 931–945. [\[CrossRef\]](#)
18. Link, O.; Brox-Escudero, L.M.; González, J.; Aguayo, M.; Torrejón, F.; Montalva, G.; Eguibar-Galán, M.Á. A paleo-hydro-geomorphological perspective on urban flood risk assessment. *Hydrol. Process.* **2019**, *33*, 3169–3183. [\[CrossRef\]](#)
19. Garreaud, R. Warm Winter Storms in Central Chile. *J. Hydrometeorol.* **2013**, *14*, 1515–1534. [\[CrossRef\]](#)
20. Lara, A.; Garcia, X.; Bucci, F.; Ribas, A. What do people think about the flood risk? An experience with the residents of Talcahuano city, Chile. *Nat. Hazards* **2016**, *85*, 1557–1575. [\[CrossRef\]](#)
21. Rojas, O.; Mardones, M.; Arumí, J.L.; Aguayo, M. Una revisión de inundaciones fluviales en Chile, período 1574–2012: Causas, recurrencia y efectos geográficos. *Rev. Geogr. Norte Gd.* **2014**, *57*, 177–192. [\[CrossRef\]](#)
22. Rojas, O.; Mardones, M.; Rojas, C.; Martínez, C.; Flores, L. Urban Growth and Flood Disasters in the Coastal River Basin of South-Central Chile (1943–2011). *Sustainability* **2017**, *9*, 195. [\[CrossRef\]](#)
23. Garreaud, R.D.; Boisier, J.P.; Rondanelli, R.; Montecinos, A.; Sepúlveda, H.H.; Veloso-Aguila, D. The Central Chile Mega Drought (2010–2018): A climate dynamics perspective. *Int. J. Clim.* **2019**, *40*, 421–439. [\[CrossRef\]](#)
24. Farooq, M.; Shafique, M.; Khattak, M.S. Flood hazard assessment and mapping of River Swat using HEC-RAS 2D model and high-resolution 12-m TanDEM-X DEM (WorldDEM). *Nat. Hazards* **2019**, *97*, 477–492. [\[CrossRef\]](#)
25. Ghimire, E.; Sharma, S. Flood Damage Assessment in HAZUS Using Various Resolution of Data and One-Dimensional and Two-Dimensional HEC-RAS Depth Grids. *Nat. Hazards Rev.* **2021**, *22*, 04020054. [\[CrossRef\]](#)
26. Rangari, V.A.; Umamahesh, N.V.; Bhatt, C.M. Assessment of inundation risk in urban floods using HEC RAS 2D. *Model. Earth Syst. Environ.* **2019**, *5*, 1839–1851. [\[CrossRef\]](#)
27. Universidad del Biobío. *Estudio de Riesgos de Sismos y Maremoto para Comunas Costeras de la Región del Biobío*; Subsecretaría de Desarrollo Regional y Administrativo del Ministerio del Interior, Gobierno de Chile/Departamento de Planificación y Diseño Urbano, Laboratorio de Estudios Urbanos, Facultad de Arquitectura, Construcción y Diseño, Universidad del Bío-Bío: Concepción, Chile, 2010.
28. Ministerio de Obras Públicas (MOP). *Reposición Puente Sobre el Río Biobío*; Ministerio de Obras Públicas (MOP): San Pedro de la Paz, Chile, 2011.
29. Van Heemst, C.; Willems, J.; Weller, A.; Van Verseveld, H.; Caamaño, D.; Aránguiz, R. Flood defense alternatives for the lower Bío Bío River, Chile. *Obras Proyectos* **2013**, *14*, 22–33. [\[CrossRef\]](#)
30. US Army Corps of Engineers (USACE). *HEC-RAS River Analysis System 2D Modeling User's Manual Version 6.0*; Davis, C.A., Ed.; USACE: Washington, DC, USA, 2021.
31. IPCC. Climate Change. Impacts, Adaptation, and Vulnerability. In *Contribution of Working Group II to the Sixth Assessment Report of the Intergovernmental Panel on Climate Change*; Pörtner, H.-O., Roberts, D.C., Tignor, M., Poloczanska, E.S., Mintenbeck, K., Alegría, A., Craig, M., Langsdorf, S., Löschke, S., Möller, V., et al., Eds.; Cambridge University Press: Cambridge, UK, 2022.
32. England, J.F., Jr.; Cohn, T.A.; Faber, B.A.; Stedinger, J.R.; Thomas, W.O., Jr.; Veilleux, A.G.; Kiang, J.E.; Mason, R.R., Jr. *Guidelines for Determining Flood Flow Frequency—Bulletin 17C (No. 4-B5)*; US Geological Survey: Reston, VA, USA, 2018.
33. Rojas, C.; Munizaga, J.; Rojas, O.; Martínez, C.; Pino, J. Urban development versus wetland loss in a coastal Latin American city: Lessons for sustainable land use planning. *Land Use Policy* **2018**, *80*, 47–56. [\[CrossRef\]](#)
34. Kron, W. Flood risk= hazard · values · vulnerability. *Water Int.* **2005**, *30*, 58–68. [\[CrossRef\]](#)
35. Farías, M.; Vargas, G.; Tassara, A.; Carretier, S.; Baize, S.; Melnick, D.; Bataille, K. Land-level changes produced by the M w 8.8 2010 Chilean earthquake. *Science* **2010**, *329*, 916–916. [\[CrossRef\]](#)
36. Gedan, K.B.; Kirwan, M.L.; Wolanski, E.; Barbier, E.B.; Silliman, B. The present and future role of coastal wetland vegetation in protecting shorelines: Answering recent challenges to the paradigm. *Clim. Chang.* **2010**, *106*, 7–29. [\[CrossRef\]](#)
37. Bywater-Reyes, S.; Diehl, R.M.; Wilcox, A.C. The influence of a vegetated bar on channel-bend flow dynamics. *Earth Surf. Dyn.* **2018**, *6*, 487–503. [\[CrossRef\]](#)
38. Bertoldi, W.; Drake, N.A.; Gurnell, A.M. Interactions between river flows and colonizing vegetation on a braided river: Exploring spatial and temporal dynamics in riparian vegetation cover using satellite data. *Earth Surf. Process. Landf.* **2011**, *36*, 1474–1486. [\[CrossRef\]](#)
39. Merritt, D.M.; Cooper, D.J. Riparian vegetation and channel change in response to river regulation: A comparative study of regulated and unregulated streams in the Green River Basin, USA. *Regul. Rivers Res. Manag.* **2000**, *16*, 543–564. [\[CrossRef\]](#)
40. Miller, K.A.; Webb, J.A.; de Little, S.C.; Stewardson, M.J. Environmental flows can reduce the encroachment of terrestrial vegetation into river channels: A systematic literature review. *Environ. Manag.* **2013**, *52*, 1202–1212. [\[CrossRef\]](#) [\[PubMed\]](#)
41. Shafroth, P.B.; Wilcox, A.C.; Lytle, D.A.; Hickey, J.T.; Andersen, D.C.; Beauchamp, V.B.; Hautzinger, A.; McMullen, L.E.; Warner, A. Ecosystem effects of environmental flows: Modelling and experimental floods in a dryland river. *Freshw. Biol.* **2010**, *55*, 68–85. [\[CrossRef\]](#)

- 
42. Grams, P.E.; Schmidt, J.C.; Topping, D.J. The rate and pattern of bed incision and bank adjustment on the Colorado River in Glen Canyon downstream from Glen Canyon Dam, 1956–2000. *GSA Bull.* **2007**, *119*, 556–575. [[CrossRef](#)]
  43. Manners, R.B.; Schmidt, J.C.; Scott, M.L. Mechanisms of vegetation-induced channel narrowing of an unregulated canyon river: Results from a natural field-scale experiment. *Geomorphology* **2014**, *211*, 100–115. [[CrossRef](#)]
  44. Pacheco, F.; Rojas, O.; Hernández, E.; Caamaño, D. Effects on Fluvial Geomorphology and Vegetation Cover following Hydroelectric Power Plant Operation: A Case Study in the Maule River (Chile). *Water* **2022**, *14*, 1673. [[CrossRef](#)]
  45. Batalla, R.J.; Iroumé, A.; Hernández, M.; Llena, M.; Mazzorana, B.; Vericat, D. Recent geomorphological evolution of a natural river channel in a Mediterranean Chilean basin. *Geomorphology* **2018**, *303*, 322–337. [[CrossRef](#)]
  46. Tabari, H.; Hosseinzadehtalaei, P.; Thiery, W.; Willems, P. Amplified Drought and Flood Risk Under Future Socioeconomic and Climatic Change. *Earth's Future*. **2021**, *9*, e2021EF002295. [[CrossRef](#)]
  47. Martínez-Fernández, V.; Van Oorschot, M.; De Smit, J.; González del Tánago, M.; Buijse, A.D. Modelling feedbacks between geomorphological and riparian vegetation responses under climate change in a Mediterranean context. *Earth Surf. Process. Landf.* **2018**, *43*, 1825–1835. [[CrossRef](#)]